Active Regulation of Pressure and Volume Defines an Energetic Constraint on the Size of Cell Aggregates

M. S. Yousafzai,[1,2,5,*] V. Yadav,[1,2,*] S. Amiri,[2,3] Y. Errami,[2,4,5] S. Amiri,[1,2] and M. Murrell[1,2,5,6†]
[1]Department of Biomedical Engineering, Yale University, 55 Prospect Street, New Haven, Connecticut 06511, USA
[2]Systems Biology Institute, Yale University, 850 West Campus Drive, West Haven, Connecticut 06516, USA
[3]Department of Mechanical Engineering and Material Science, Yale University, 10 Hillhouse Avenue, New Haven, Connecticut 06511, USA
[4]Department of Genetics, Yale School of Medicine, Sterling Hall of Medicine, 333 Cedar Street, New Haven, Connecticut 06510, USA
[5]Center for Cancer Systems Biology, Yale University, 850 West Campus Drive, West Haven, Connecticut 06516, USA
[6]Department of Physics, Yale University, 217 Prospect Street, New Haven, Connecticut 06511, USA

(Received 9 February 2021; accepted 3 January 2022; published 28 January 2022)

We explore the relationship between the nonequilibrium generation of myosin-induced active stress within the *F*-actin cytoskeleton and the pressure-volume relationship of cellular aggregates as models of simple tissues. We find that due to active stress, aggregate surface tension depends upon its size. As a result, both pressure and cell number density depend on size and violate equilibrium assumptions. However, the relationship between them resembles an equilibrium equation of state with an effective temperature. This suggests that bulk and surface properties of aggregates balance to yield a constant average work performed by each cell on their environment in regulating tissue size. These results describe basic physical principles that govern the size of cell aggregates.

DOI: 10.1103/PhysRevLett.128.048103

The regulation of pressure and volume in cells involves the coordination between nonequilibrium "active" stresses generated by the actomyosin cytoskeleton [1,2] and diverse mechanosensitive processes in the cell, such as fluid and solute flow through pores and gated ion channels [3–6]. This leads to a dynamic force balance between elastic and fluid stresses, which will determine the shape of cells and tissues [7–11]. For example, active stresses elevate intracellular hydrostatic pressure to drive cell rounding and determine cell volume during cytokinesis [12–15]. By contrast, active stresses within tissues induce intercellular fluid flow through gap junctions in the epithelium [16] that lead to large volume fluctuations across the tissue [17,18]. Thus, while active stresses drive reciprocal changes in pressure and volume within cells, the constraints on these changes are unclear.

In equilibrium, the relationship between pressure, volume, temperature, and other state variables is described by an equation of state [19]. For example, an equation of state for an ideal gas constrains changes in pressure and volume such that their product is a thermodynamic work. By contrast, out of equilibrium, these constraints may not hold. Inhomogeneities or nonintensivity in thermodynamic variables violate equilibrium assumptions and suggest that no equation of state exists [20–23]. For example, in living cells, the presence of active stress within the cell cytoskeleton leads to inhomogeneities and nonequilibration in cellular pressure [24–29]. In this case, intracellular pressure may include contributions from the hydraulic pressure in cytosol, effects of nondeviatoric stresses in the cytoskeleton, and partial pressures related to solute concentrations. Thus, while many variables may be involved in characterizing the nonequilibrium state, the extent that work constrains pressure and volume changes far from equilibrium is not known.

In this Letter, we explore the role of nonequilibrium active stress generated by myosin molecular motors on the surface tension of cellular aggregates, as models of simple tissues. We show that with varying aggregate size, these variables are nonintensive and violate equilibrium assumptions. However, in combination, the relationship between them defines an energetic constraint on the production of work away from equilibrium. This constraint may constitute a fundamental principle that relates the size and mechanics of cellular aggregates.

Aggregates of S180 sarcoma cells are formed through suspension spinning and are between 50 and 225 μm in radius (Supplemental Material, Figure 1 [30]) [31]. They are spherical in shape and have a smooth surface. The *F*-actin cytoskeleton is visualized using *F*-Tractin staining, which outlines the shape of the cells within the aggregate [Fig. 1(a)]. Further, the nuclei of the cells are visualized with green fluorescence protein (GFP) tagged with a nuclear localization sequence (NLS), which enables an estimation of the number density of cells, and their orientation within the aggregate as all cells are mononucleated [Fig. 1(b), Supplemental Material [30]) [32,33].

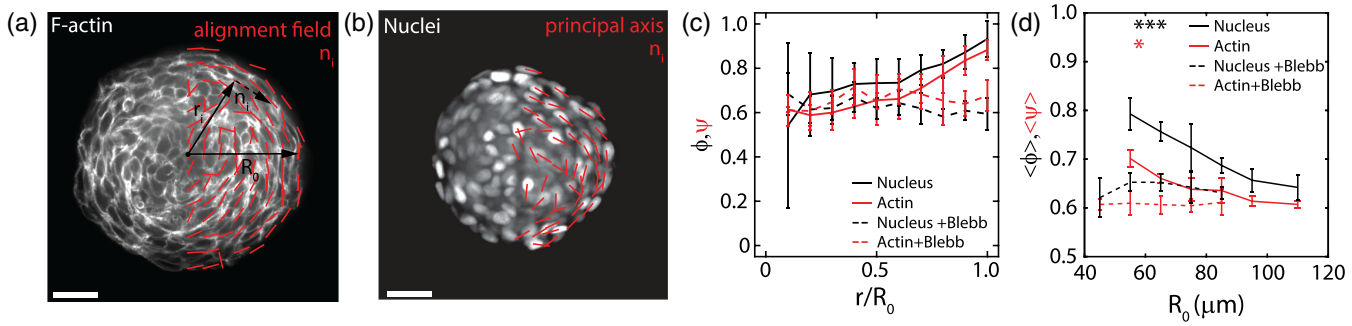

FIG. 1. Aggregates exhibit size-dependent cytoskeletal organization. (a) Fluorescently labeled F-actin and (b) fluorescently labeled nuclei at an equatorial plane of an aggregate. Red lines in (a) and (b) denote F-actin alignment ($\hat{n}$) and nuclei orientation respectively ($\hat{n}_i$). (c) Radially averaged orthoradial ordering (ϕ) as measured from F-actin alignment (defined as $\phi = \langle|\hat{r}_i \times \hat{n}_i|\rangle$) (red) and from nuclei deformation (black), as a function of distance from the aggregate center r normalized by the radius of aggregate R_0 ($n = 8$). (d) Mean orthoradial ordering for actin orientation and nucleus deformation is size dependent ($n = 23$). Dashed red and black lines in panels (c) and (d) denote orthoradial ordering in actin and nuclei respectively, in Blebbistatin-treated aggregates. The scale bar is 50 μm. Error bars are mean $\pm$ standard deviation. $^{***}P < 0.001$, $^{*}P < 0.05$.

First, we observe a radial organization of F-actin, and nuclear deformation from the outer surface of the aggregate into the inner core. At the surface, the F-actin is more aligned, while at the center of the aggregate, the F-actin is more disordered. This suggests that cells are more polarized and elongated at the surface than in the center. To quantify this, we define a scalar order parameter ϕ, given by $\langle|\hat{r}_i \times \hat{n}_i|\rangle$, where $\hat{r}_i$ and $\hat{n}_i$ are the unit position vector to a point inside the aggregate and the corresponding F-actin orientation field at that location, respectively [Fig. 1(a)]. We show that ϕ decreases from the surface of the aggregate ($r = R_0$) toward the core ($r = 0$), until it reaches a steady value, at approximately half the aggregate radius [Fig. 1(c)].

Second, like the F-actin organization we also observe a radial dependence to nuclear shape, as represented by vectors indicating the axis of elongation [Fig. 1(b)]. The nuclei are more elongated on the surface, and rounder in the center, consistent with previous results [34–36]. The elongation can be represented similarly as F-actin alignment, by the scalar order parameter ψ, where ψ has the same functional form as ϕ, with $\hat{n}_i$ now representing the unit orientation vector of the long axis of the nuclei. We note that the gradients in the order parameters are similar in magnitude for actin and nuclei alignment [Fig. 1(c)].

When averaged over the radial dimension of the aggregates ($0 \leq r \leq R_0$), the scalar order parameters show a size-dependent response [Fig. 1(d)]. Both ϕ and ψ are indicative of the state of internal active stress, as F-actin alignment correlates to the generation of active stresses. This is consistent with previous Letter that shows a pressure profile in cell aggregates; thus the elongation of nuclei may indicate that they are deformed, and therefore reflect the application of those stresses [34–38]. However, the scalar order parameter is constant in the orthoradial direction and implies that anisotropy in the radial direction does not lead to anisotropy on the surface (Supplemental Material Fig. 1).

Upon inhibition of active stress by 50 μM Blebbistatin, a myosin ATPase inhibitor [39], all size dependence is lost, both in F-actin alignment and nuclear deformation [Figs. 1(c) and 1(d)].

As noted, the alignment of F-actin and the elongation of nuclei may be representative of a higher level of active stress at the surface. By contrast, a lower level of alignment and round nuclei in the center may be representative of internal pressure. These observations suggest size-dependent surface tension and pressure. However, an alternative includes the possibility of differential cytoskeletal assembly at the periphery, unrelated to the mechanics of the aggregate. To test the hypothesis that alignment and deformation are consistent with size-dependent mechanics, we measure the surface tension of cellular aggregates by micropipette aspiration.

Using micropipette aspiration we apply creep and stress relaxation tests to estimate the surface tension of the aggregate [Figs. 2(a) and 2(b), Supplemental Material Figs. 3 and 4, Supplemental Material Notes 1 and 2 [30]) [40]. To measure these quantities we perform aspiration experiments on aggregates of different sizes (hence a different number of constituent cells N and different volume V). Briefly, a negative step pressure is applied to the pipette for 1 h (τ_{exp}) which draws the aggregate into the pipette a length L [Fig. 2(b)]. L will increase over time until the pressure is released, at which point L decreases over 1 h. By fitting the L-t data with a modified Maxwell model, we calculate the effective stiffness E_{eff} and the viscosity η of the aggregate to be 500 Pa, and 2×10^5 Pa s, respectively. The viscoelastic time scale is then defined as $\tau_v = \eta/E_{\text{eff}} = 400$ s.

As $\tau_{\text{exp}} \gg \tau_v$, the aggregate surface behaves as a fluid, and thus we assume that the deviatoric component of the stress tensor is negligible [Fig. 2(c)]. This is consistent with the lack of aforementioned variations in F-actin ordering

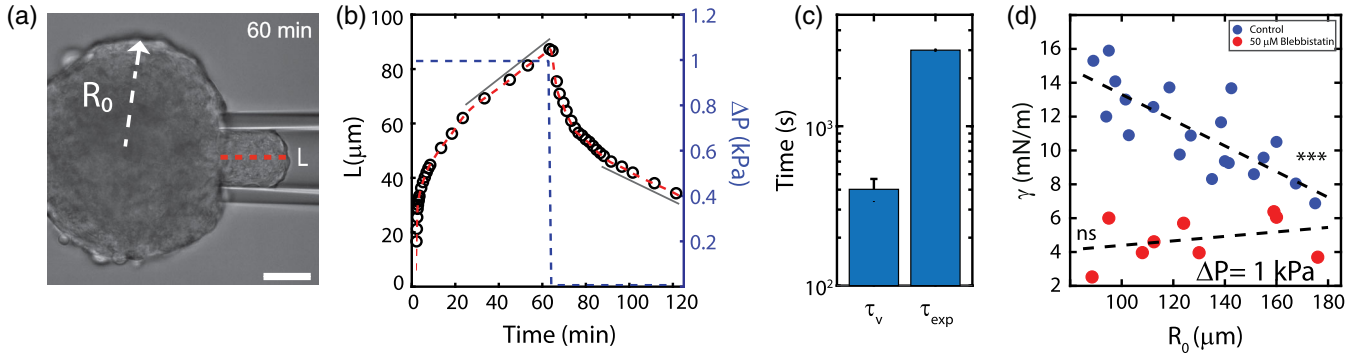

FIG. 2. Aggregate surface tension is size-dependent. (a) Brightfield image of micropipette aspiration which shows the aggregate entering the pipette over a length L (indicated by dotted red line). (b) L over time (black circles, dotted red line). A step increase in pressure is applied and then released at the apex of L (blue dotted line). Solid gray lines represent the region where aspiration and retraction rates are measured. This region represents a fluid like regime. (c) Comparison between viscoelastic and experimental time scales. (d) Surface tension γ as a function of aggregate size, R_0, for control ($n = 21$, blue) and 50 μM Blebbistatin-treated aggregates (n = 9, red). $^{***}P < 0.001$ ns is nonsignificant. Scale bar is 50 μm. Error bars are mean $\pm$ standard deviation.

along the aggregate surface. Relatedly, we also show that no surface flows are observed, suggesting that no surface tension gradient exists (Supplemental Material Note 3 and Supplemental Material Fig. 5 [30]). Therefore, we assume that γ is isotropic. Thus, in absence of anisotropy in stress gradients in a fluid regime, we apply the law of Laplace to connect surface tension with pressure (Supplemental Material Notes 3 and 4). Separately, a Laplace-like relationship has been observed during aggregate adhesion [31] and is utilized in studies of aggregate mechanics [10,40,41].

From the change of L in time, and application of the law of Laplace, we calculate the surface tension γ of the aggregate [Fig. 2(d), Video 1] [40]. First, we find that γ is 14.32 ± 1.72 mN/m, consistent with previous reports [40,41]. However, we also find that γ decreases with an increase in aggregate size, indicating that small aggregates have a larger surface tension (14.32 ± 1.72 mN/m) than large ones (7.46 ± 0.83 mN/m). The decrease in surface tension as a function of aggregate size can be treated as linear over aggregate size range explored in this study ($d\gamma/dR_0 = -76.0 \pm 13.8$ N/m^2). Thus, as the pipette retains a fixed diameter, aggregates of different sizes are deformed to the same length scale, yet have different surface tensions. This implies that aggregates of different sizes act as droplets of fluids with different surface tensions. Furthermore, upon treatment with 50 μM Blebbistatin, the size dependence vanishes ($d\gamma/dR_0 = 13.2 \pm 15.5$ N/m^2), consistent with that of passive systems, like liquid droplets [42–44]. These results are also consistent with results that do not assume Laplace (Supplemental Material Note 5, and Supplemental Material Fig. 6 [30])[45,46].

Next, we calculate the internal pressure (P) and volume (V) of the aggregate from the micropipette aspiration experiments. To do so, we apply the law of Laplace for a droplet, i.e., $P = 2\gamma/R_0$, using the measured γ from micropipette, and the curvatures as measured from brightfield images. To measure the volume, we assume radial symmetry of the brightfield images, and convert measurements of the area into estimates of volume. Under the assumption that the final state of an aggregate is independent of how it was prepared, aggregates of different sizes may mimic a continuously growing aggregate.

Comparing these measurements, we find an inverse relationship between the pressure and volume [Fig. 3(a)]. Small aggregates have high surface tension and likewise, have high internal pressure. By contrast, large aggregates have low surface tension and thereby low pressure. Specifically, by fitting pressure and volume data, we find that $P \sim V^{-0.6\pm0.11}$, or $P \sim R_0^{-1.8\pm0.32}$. This relationship is dependent upon active stress, as in the presence of 50 μM Blebbistatin, the aggregate increases in volume and maintains a round shape [Fig. 3(a), inset]. Further, as the concentration of myosin scales as R_0^{-1} (Supplemental Material Fig. 7) and γ is proportional to myosin content, the law of Laplace would suggest that for aggregates pressure should follow a $P \sim R_0^{-2}$ dependence as opposed to $P \sim R_0^{-1}$ in the case of a passive drop. As $R_0 \sim V^{1/3}$, writing pressure in terms of aggregate volume gives $P \sim V^{-2/3}$, which agrees with experimental data.

An activity-dependent change in aggregate volume indicates a change in the number density of cells within the aggregate [47,48]. By transfecting cells for GFP with NLS, we estimated the population of cells (N) and thereby the cell number density ($\rho = N/V$) within the aggregate. From images of nuclei, we estimate the cell number density in two different ways based on the size of the aggregate relative to the field of view (Supplemental Material Notes 6 and 7, Supplemental Material Fig. 8, Supplemental Material Video 2 [30]). First, for small aggregates ($R_0 < 100$ μm), we spread aggregates onto adhesive substrates and count the nuclei that enter the two-dimensional plane until the aggregate completely depletes. We then estimate the initial volume (V) from a brightfield image of

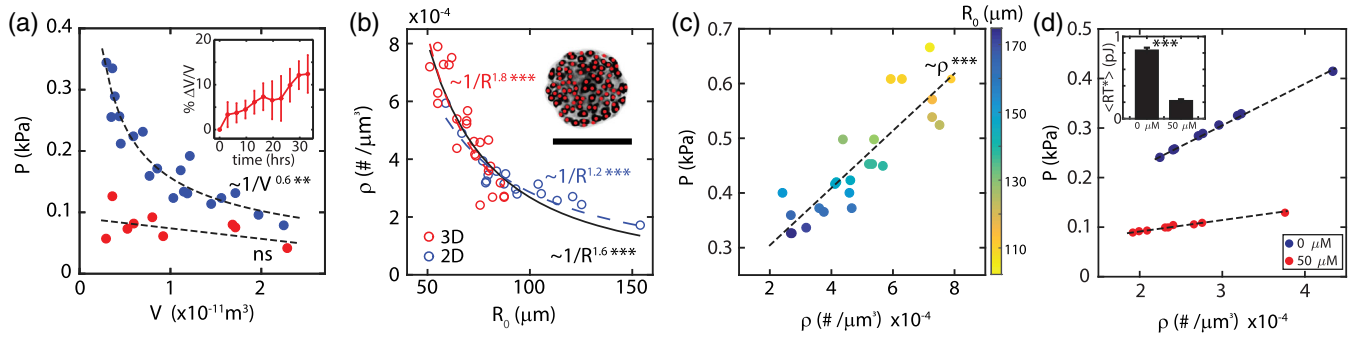

FIG. 3. Pressure and cell number density are both size dependent yielding constant work. (a) Pressure-volume relationship for different aggregates of multiple sizes (blue, no treatment; red, treated with 50 μM Blebbistatin). Inset: volume expansion of a nonadherent aggregate in 50 μM Blebbistatin. (b) Cell number density (ρ), as measured through nuclei counting, decreases with the increasing size of the aggregate. Inset: inverted fluorescence image of nuclei of an aggregate with red dots that identify their fluorescent centers. (c) Aggregate pressure and number density are linearly correlated and inversely proportional to the aggregate size. (a)–(c) Each point represents a single experiment. (d) Pressure and number density relationship for different levels of active stress. RT^* for 0 and 50 μM Blebbistatin (d, inset). $^{***}P < 0.001$. $^{**}P < 0.01$ ns is nonsignificant. Scale bar is 100 μm. Error bars are mean $\pm$ standard deviation.

the cross section of the aggregate prior to spreading, and normalize the population by this volume. Separately, for large aggregates ($R_0 > 100$ μm), we cannot see all spread cells within a single field of view, and thus count nuclei within a 2D confocal slice. Therefore we convert the 2D number density to 3D by assuming a uniform distribution of cells. We find that the former method yields $\rho \sim R_0^{-1.8\pm0.29}$ for small aggregates, the latter gives $R_0^{-1.2}$ for large aggregates, and for the whole range, $R_0^{-1.6\pm0.26}$ [Fig. 3(b)]. Over the size of aggregates used in this study, these number density changes correspond to changes in average cell volume up to a factor of 3.0 ± 0.4 which is comparable to other studies [16,49,50]. However, other studies have suggested that cytoskeletal-mediated volume change is not entirely through direct mechanical actuation of volume by cytoskeletal forces but through water permeation from pores and gated ion channels [51], as the shear modulus of the cell is orders of magnitude smaller than the bulk modulus of the cell. Thus, there may be a complex interaction involving both mechanics and signaling between ion channels and the cytoskeleton that mediate these effects [16,52].

The scaling of pressure with aggregate size ($P \sim R_0^{-1.8\pm0.29}$) is comparable to the scaling of number density with size ($\rho \sim R_0^{-1.6\pm0.26}$) (Supplemental Material Note 8 [30]). The exponent of the fit matches precisely for the more accurate estimate for small aggregates ($R_0 \leq 100\,\mu$m). The R^2 value for power law fits for small aggregates (0.84) is also observed to be significantly better that for the complete data set (0.69). Thus, when normalizing the product of pressure and volume for each aggregate by the population of cells within each aggregate (PV/N, or equivalently P/ρ), we find that the average energy contributed per cell remains constant [Fig. 3(c)]. This is expected for a density scaling of R_0^{-2}, similar to small R_0 measurements (Supplemental Material Fig. 8 [30]). Thus, assuming that the exponents are indistinguishable, the relationship between pressure and number density resembles an equilibrium equation of state of form

$$\frac{P}{\rho} = \langle W \rangle = \tilde{R} T^*. \tag{1}$$

For increasing size and cell density, $\langle W \rangle$ denotes the mean mechanical and nonmechanical energetic cost of adding a cell to the aggregate, T^* is an effective temperature which is a measure of the activity of an aggregate, and $\tilde{R}$ is a constant. Upon reduction of the active stress through myosin inhibition, the linear relationship remains, although T^* is lowered [Fig. 3(d)]. Thus T^* is related to the internal, nonequilibrium activity of the cell. By contrast, a difference in the scaling exponents in P and ρ may lead to an exponent of $V^{1.13}$ as aggregates become larger and thus temperature is not constant in the limit of large aggregates (Supplemental Material Note 9 [30]).

The slope of the $P - \rho$ curve reflects the effective thermodynamic temperature. Equating the slope of $P - \rho$ curve with $k_B T$ yields a temperature of the order $\approx 10^{11}$ K (1 pJ). For the Blebbistatin-treated case this estimate is approximately $\approx 10^{10}$ K (0.1 pJ). Such large values are expected, as cellular aggregates are athermal systems. Similarly large values have been observed in granular materials ($\approx 10^{13}$ K) [53]. However, as the range of cell number densities covered by aggregates of different sizes in this study is much larger than the change in density of a single aggregate on inhibition of myosin activity, we infer that T^* includes contributions from other sources, in addition to myosin activity [Fig. 3(a) inset, Supplemental Material Note 10 [30]). Thus while more variables may be required to completely specify the state of an aggregate, the

pressure-density relationship is still sufficient to define an energetic constraint on the size of cell aggregates.

Previous reports have estimated the energetic cost of S180 cell adhesion to be approximately 40 $\mu J/m^2$, or $\sim 1 \times 10^{-3}$ pJ given the size of the cell [54]. To estimate the contribution of active stress, we measure changes in traction strain energy as single cells de-adhere from a compliant substrate to form an aggregate. Thus, we seed single S180 cells on a 0.7 kPa polyacrylamide gel, coated with 10 $\mu g/mL$ fibronectin. As the fibronectin concentration is low, as cells migrate and contact each other, the cohesion between them will induce substrate de-adhesion and aggregation (Supplemental Material Fig. 9 [30]). The formation of the aggregate is favorable, and thus the loss in traction strain energy reflects a lower bound on the active stresses generated in the formation of the aggregate itself. In our experiments this value is 5×10^{-3} pJ, and has been observed to be as high as 0.1 pJ in other experiments reported in literature [55]. To estimate a contribution to the pressure-volume work, we apply an osmotic pressure of 400 Pa to nonadherent S180 cells, and measure a change of volume of 7%, yielding an estimated work of $\sim$0.1 pJ, comparable to our estimates (Supplemental Material Note 11 [30]).

In passive liquid droplets, pressure varies with size exclusively due to droplet curvatures, as described by the law of Laplace. In cellular aggregates, the law of Laplace holds as the surface tension is isotropic. Here we show that in aggregates as models of active droplets, pressure also depends on size, although due to a volume-dependent surface tension arising from active stress. By extension, pressure or number density may not uniquely define the state of the system. However, pressure and number density vary similarly with size and thus in the relationship between them, this dependence vanishes, and resembles an equation of state. Here, the nonequilibrium activity can be represented as an athermal temperature as is observed in granular systems, active colloids, and turbulent fluids [56–58]. Thus while single variables violate equilibrium assumptions, in combination, these variables may still define a work and constrain the energetics of the system.

In ideal gases, the equation of state appears due to the noninteractivity between constituent particles. By contrast in cell aggregates, the relationship between pressure and density is due to the presence of active interactions and adhesions that enables pressure and number density to have similar scaling with the size of the aggregate. As aggregates of different cell lines also show a similar size-dependent response, we suggest that these results may be general (Supplemental Material Fig. 10 [30]).

As the size of the aggregate grows, the simple linear equation of state may need a more complex functional form or the addition of higher-order virial terms. We briefly discuss modifications to this relationship in the Supplemental Material, and we plan to explore this idea in future works (Supplemental Material Note 9 [30]).

Overall, we show that the bulk and surface properties of the cell aggregate balance to yield a constant work for aggregates of different sizes. The study presented here may represent new insights for understanding the growth and form of simple tissues, and the regulation of energy far from equilibrium in living systems.

We acknowledge funding ARO MURI W911NF-14-1-0403 to M. M. and V. Y. as well as National Institute of Health (NIH) RO1 GM126256 to M. M. and NIH U54 CA209992 to M. M. and M. S. Y. M. M. also acknowledges support from Human Frontiers Science Program (HFSP) Grant No. RGY0073/2018. Any opinion, findings, and conclusions or recommendations expressed in this material are those of the authors(s) and do not necessarily reflect the views of the DoD, NIH, or HFSP. We would like to thank Prof. Erdem Karatekin for help with micropipette measurements. We would also like to thank Dr. Karine Guevorkian, Professor Francoise Brochard-Wyart, Dr. Rob Style, and Dr. Daniel Seara for constructive discussion. M. M. designed and conceived the work. M. M. drafted the paper. M. S. Y. and S. A. acquired experimental data. M. M., M. S. Y., V. Y., and S. A. analyzed experimental data. M. M. and V. Y. edited the paper.

*These authors contributed equally to this work.
†Corresponding author.
michael.murrell@yale.edu

[1] M. Murrell, P. W. Oakes, M. Lenz, and M. L. Gardel, Forcing cells into shape: The mechanics of actomyosin contractility, Nat. Rev. Mol. Cell Biol. **16**, 486 (2015).
[2] M. Das, C. F. Schmidt, and M. Murrell, Introduction to active matter, Soft Matter **16**, 7185 (2020).
[3] C. A. M. La Porta, E. Monzani, F. Facchetti, and C. Perego, Knock down of AQP1 in HMEC-1 cells and WM115 cells changes the organisation of the cytoskeleton, FASEB J. **22** (2008).
[4] E. Monzani, R. Bazzotti, C. Perego, and C. A. M. La Porta, AQP1 is not only a water channel: It contributes to cell migration through lin7/beta-catenin, PLoS One **4**, e6167 (2009).
[5] S. P. O'Hara, G. B. Gajdos, B. Q. Huang, P. L. Splinter, X. M. Chen, and N. F. LaRusso, M1171 Myosin II-dependent membrane translocation of SGLT1 and AQP1 is required for efficient *C. parvum* cellular invasion of cholangiocytes, Gastroenterology **134**, A353 (2008).
[6] K. M. Stroka, H. Jiang, S. H. Chen, Z. Tong, D. Wirtz, S. X. Sun, and K. Konstantopoulos, Water permeation drives tumor cell migration in confined microenvironments, Cell **157**, 611 (2014).
[7] H. Jiang and S. X. Sun, Cellular pressure and volume regulation and implications for cell mechanics, Biophys. J. **105**, 609 (2013).
[8] A. Taloni, E. Kardash, O. U. Salman, L. Truskinovsky, S. Zapperi, and C. A. M. La Porta, Volume Changes During

Active Shape Fluctuations in Cells, Phys. Rev. Lett. **114**, 208101 (2015).
[9] J. X. Tao and S. X. Sun, Active biochemical regulation of cell volume and a simple model of cell tension response, Biophys. J. **109**, 1541 (2015).
[10] D. Gonzalez-Rodriguez, K. Guevorkian, S. Douezan, and F. Brochard-Wyart, Soft matter models of developing tissues and tumors, Science **338**, 910 (2012).
[11] B. I. Shraiman, Mechanical feedback as a possible regulator of tissue growth, Proc. Natl. Acad. Sci. U.S.A. **102**, 3318 (2005).
[12] M. P. Stewart, J. Helenius, Y. Toyoda, S. P. Ramanathan, D. J. Muller, and A. A. Hyman, Hydrostatic pressure and the actomyosin cortex drive mitotic cell rounding, Nature (London) **469**, 226 (2011).
[13] N. C. Gauthier, O. M. Rossier, A. Mathur, J. C. Hone, and M. P. Sheetz, Plasma membrane area increases with spread area by exocytosis of a GPI-anchored protein compartment, Mol. Biol. Cell **20**, 3261 (2009).
[14] N. C. Gauthier, T. A. Masters, and M. P. Sheetz, Mechanical feedback between membrane tension and dynamics, Trends Cell Biol. **22**, 527 (2012).
[15] N. C. Gauthier, M. A. Fardin, P. Roca-Cusachs, and M. P. Sheetz, Temporary increase in plasma membrane tension coordinates the activation of exocytosis and contraction during cell spreading, Proc. Natl. Acad. Sci. U.S.A. **108**, 14467 (2011).
[16] E. McEvoy, Y. L. Han, M. Guo, and V. B. Shenoy, Gap junctions amplify spatial variations in cell volume in proliferating tumor spheroids, Nat. Commun. **11**, 6148 (2020).
[17] S. Zehnder, M. Suaris, M. Bellaire, and T. Angelini, Cell volume fluctuations in MDCK monolayers, Biophys. J. **108**, 247 (2015).
[18] S. M. Zehnder, F. M. Zegers, and T. E. Angelini, A langevin model of physical forces in cell volume fluctuations, J. Biomech. **49**, 1286 (2016).
[19] L. Landau and E. Lifshitz, *Statistical Physics* (Butterworth-Heinemann, London, 2013).
[20] A. P. Solon, Y. Fily, A. Baskaran, M. E. Cates, Y. Kafri, M. Kardar, and J. Tailleur, Pressure is not a state function for generic active fluids, Nat. Phys. **11**, 673 (2015).
[21] F. Ginot, I. Theurkauff, D. Levis, C. Ybert, L. Bocquet, L. Berthier, and C. Cottin-Bizonne, Nonequilibrium Equation of State in Suspensions of Active Colloids, Phys. Rev. X **5**, 011004 (2015).
[22] E. Bertin, O. Dauchot, and M. Droz, Definition and Relevance of Nonequilibrium Intensive Thermodynamic Parameters, Phys. Rev. Lett. **96**, 120601 (2006).
[23] G. Junot, G. Briand, R. Ledesma-Alonso, and O. Dauchot, Active Versus Passive Hard Disks Against a Membrane: Mechanical Pressure and Instability, Phys. Rev. Lett. **119**, 028002 (2017).
[24] E. Moeendarbary, L. Valon, M. Fritzsche, A. R. Harris, D. A. Moulding, A. J. Thrasher, E. Stride, L. Mahadevan, and G. T. Charras, The cytoplasm of living cells behaves as a poroelastic material, Nat. Mater. **12**, 253 (2013).
[25] T. J. Mitchison, G. T. Charras, and L. Mahadevan, Implications of a poroelastic cytoplasm for the dynamics of animal cell shape, Semin. Cell Dev. Biol. **19**, 215 (2008).
[26] G. T. Charras, J. C. Yarrow, M. A. Horton, L. Mahadevan, and T. J. Mitchison, Non-equilibration of hydrostatic pressure in blebbing cells, Nature (London) **435**, 365 (2005).
[27] G. T. Charras, M. Coughlin, T. J. Mitchison, and L. Mahadevan, Life and times of a cellular bleb, Biophys. J. **94**, 1836 (2008).
[28] G. Charras and E. Paluch, Blebs lead the way: How to migrate without lamellipodia, Nat. Rev. Mol. Cell Biol. **9**, 730 (2008).
[29] J.-Y. Tinevez, U. Schulze, G. Salbreux, J. Roensch, J.-F. Joanny, and E. Paluch, Role of cortical tension in bleb growth, Proc. Natl. Acad. Sci. U.S.A. **106**, 18581 (2009).
[30] See Supplemental Material at http://link.aps.org/supplemental/10.1103/PhysRevLett.128.048103 for additional data and methodology description.
[31] M. S. Yousafzai, V. Yadav, S. Amiri, M. Staddon, A. P. Tabatabai, Y. Errami, G. Jaspard, S. Amiri, S. Banerjee, and M. Murrell, Tissue pressure and cell traction compensate to drive robust aggregate spreading, bioRxiv (2020) 10.1101/2020.08.29.273334.
[32] D. S. Seara, V. Yadav, I. Linsmeier, A. P. Tabatabai, P. W. Oakes, S. M. A. Tabei, S. Banerjee, and M. P. Murrell, Entropy production rate is maximized in non-contractile actomyosin, Nat. Commun. **9**, 4948 (2018).
[33] M. Cetera, G. R. Ramirez-San Juan, P. W. Oakes, L. Lewellyn, M. J. Fairchild, G. Tanentzapf, M. L. Gardel, and S. Horne-Badovinac, Epithelial rotation promotes the global alignment of contractile actin bundles during *Drosophila* egg chamber elongation, Nat. Commun. **5**, 5511 (2014).
[34] M. E. Dolega, M. Delarue, F. Ingremeau, J. Prost, A. Delon, and G. Cappello, Cell-like pressure sensors reveal increase of mechanical stress towards the core of multicellular spheroids under compression, Nat. Commun. **8**, 14056 (2017).
[35] M. Dolega, G. Zurlo, M. L. Goff, M. Greda, C. Verdier, J.-F. Joanny, G. Cappello, and P. Recho, Mechanical behavior of multi-cellular spheroids under osmotic compression, J. Mech. Phys. Solids **147**, 104205 (2021).
[36] M. Delarue, J. F. Joanny, F. Julicher, and J. Prost, Stress distributions and cell flows in a growing cell aggregate, Interface Focus **4**, 20140033 (2014).
[37] M. C. Marchetti, J. F. Joanny, S. Ramaswamy, T. B. Liverpool, J. Prost, M. Rao, and R. A. Simha, Hydrodynamics of soft active matter, Rev. Mod. Phys. **85**, 1143 (2013).
[38] J. F. Joanny, F. Julicher, K. Kruse, and J. Prost, Hydrodynamic theory for multi-component active polar gels, New J. Phys. **9**, 422 (2007).
[39] M. Kovacs, J. Toth, C. Hetenyi, A. Malnasi-Csizmadia, and J. R. Sellers, Mechanism of blebbistatin inhibition of myosin II, J. Biol. Chem. **279**, 35557 (2004).
[40] K. Guevorkian, M. J. Colbert, M. Durth, S. Dufour, and F. Brochard-Wyart, Aspiration of Biological Viscoelastic Drops, Phys. Rev. Lett. **104**, 218101 (2010).
[41] K. Guevorkian, D. Gonzalez-Rodriguez, C. Carlier, S. Dufour, and F. Brochard-Wyart, Mechanosensitive shivering of model tissues under controlled aspiration, Proc. Natl. Acad. Sci. U.S.A. **108**, 13387 (2011).

[42] E. Y. Bormashenko, *Physics of Wetting- Phenomena and Applications of Fluids on Surfaces* (De Gruyter, Berlin, 2017).
[43] P.-G. de Gennes, F. Brochard-Wyart, and D. Querena, *Capillarity and Wetting Phenomena- Drops, Bubbles, Pearls, Waves* (Springer-Verlag, New York, New York, 2004).
[44] M. P. Murrell, R. Voituriez, J.-F. Joanny, P. Nassoy, C. Sykes, and M. L. Gardel, Liposome adhesion generates traction stress, Nat. Phys. **10**, 163 (2014).
[45] J. Frenkel, Viscous flow of crystalline bodies under the action of surface tension, J. Phys. (Moscow) **9**, 13 (1945).
[46] O. Pokluda, C. Bellehumeur, and J. Vlachopoulos, Modification of Frenkel's model for sintering, AIChE J. **43**, 3253 (1997).
[47] B. M. Bijonowski, S. I. Daraiseh, X. Yuan, and T. Ma, Size-dependent cortical compaction induces metabolic adaptation in mesenchymal stem cell aggregates, Tissue Eng. Part A **25**, 575 (2019).
[48] K. C. Murphy, B. P. Hung, S. Browne-Bourne, D. Zhou, J. Yeung, D. C. Genetos, and J. K. Leach, Measurement of oxygen tension within mesenchymal stem cell spheroids, J. R. Soc. Interface **14**, 20160851 (2017).
[49] Y. Okada, Ion channels and transporters involved in cell volume regulation and sensor mechanisms, Cell Biochem. Biophys. **41**, 233 (2004).
[50] A. Cartagena-Rivera, J. Logue, C. Waterman, and R. Chadwick, Actomyosin cortical mechanical properties in nonadherent cells determined by atomic force microscopy, Biophys. J. **110**, 2528 (2016).
[51] Y. L. Han, A. F. Pegoraro, H. Li, K. Li, Y. Yuan, G. Xu, Z. Gu, J. Sun, Y. Hao, S. K. Gupta, Y. Li, W. Tang, H. Kang, L. Teng, J. J. Fredberg, and M. Guo, Cell swelling, softening and invasion in a three-dimensional breast cancer model, Nat. Phys. **16**, 101 (2020).
[52] H. Jiang and S. Sun, Cellular pressure and volume regulation and implications for cell mechanics, Biophys. J. **105**, 609 (2013).
[53] C. Song, P. Wang, and H. A. Makse, Experimental measurement of an effective temperature for jammed granular materials, Proc. Natl. Acad. Sci. U.S.A. **102**, 2299 (2005).
[54] D. Cuvelier, M. Théry, Y.-S. Chu, S. Dufour, J.-P. Thiéry, M. Bornens, P. Nassoy, and L. Mahadevan, The universal dynamics of cell spreading, Curr. Biol. **17**, 694 (2007).
[55] J. P. Butler, I. M. Tolić-Nørrelykke, B. Fabry, and J. J. Fredberg, Traction fields, moments, and strain energy that cells exert on their surroundings, Am. J. Physiol. Cell Physiol. **282**, C595 (2002).
[56] A. Mehta, *Interdisciplinary Granular Matter* (Springer, New York, NY, New York, 1994).
[57] M. Han, J. Yan, S. Granick, and E. Luijten, Effective temperature concept evaluated in an active colloid mixture, Proc. Natl. Acad. Sci. U.S.A. **114**, 7513 (2017).
[58] M. C. Cross and P. C. Hohenberg, Pattern formation outside of equilibrium, Rev. Mod. Phys. **65**, 851 (1993).